
Generalizing Weather Forecast to Fine-grained Temporal Scales via Physics-AI Hybrid Modeling

Wanghan Xu

Shanghai AI Laboratory
xuwanghan@pjlab.org.cn

Fenghua Ling

Shanghai AI Laboratory
lingfenghua@pjlab.org.cn

Wenlong Zhang

Shanghai AI Laboratory
zhangwenlong@pjlab.org.cn

Tao Han

Shanghai AI Laboratory
hantao.dispatch@pjlab.org.cn

Hao Chen

Shanghai AI Laboratory
chenhao1@pjlab.org.cn

Wanli Ouyang

Shanghai AI Laboratory
ouyangwanli@pjlab.org.cn

Lei Bai †

Shanghai AI Laboratory
bailei@pjlab.org.cn

Abstract

Data-driven artificial intelligence (AI) models have made significant advancements in weather forecasting, particularly in medium-range and nowcasting. However, most data-driven weather forecasting models are black-box systems that focus on learning data mapping rather than fine-grained physical evolution in the time dimension. Consequently, the limitations in the temporal scale of datasets prevent these models from forecasting at finer time scales. This paper proposes a physics-AI hybrid model (i.e., WeatherGFT) which **Generalizes** weather forecasts to **Finer-grained Temporal** scales beyond training dataset. Specifically, we employ a carefully designed PDE kernel to simulate physical evolution on a small time scale (e.g., 300 seconds) and use a parallel neural networks with a learnable router for bias correction. Furthermore, we introduce a lead time-aware training framework to promote the generalization of the model at different lead times. The weight analysis of physics-AI modules indicates that physics conducts major evolution while AI performs corrections adaptively. Extensive experiments show that WeatherGFT trained on an hourly dataset, *achieves state-of-the-art performance across multiple lead times and exhibits the capability to generalize 30-minute forecasts*. Code is available at <https://github.com/black-yt/WeatherGFT>.

1 Introduction

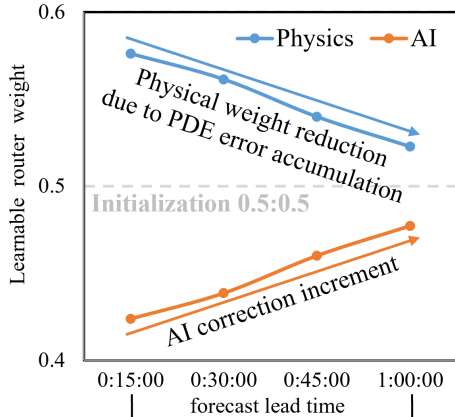
Weather forecasting plays a vital role in modern society, impacting a wide range of human activities. For example, minute-level precipitation nowcasting is particularly valuable for short-term planning, such as outdoor activities, while medium-range forecasts that offer daily predictions play a crucial role in long-term strategic decisions like maritime trade. This field has witnessed remarkable advancements in recent years, largely attributed to the rapid progress of machine learning-based (ML) weather forecasting models [33], spanning from nowcasting to medium-range forecasts.

Prior studies tackle the problem of weather forecasting by leveraging data-driven models trained on benchmark weather forecasting datasets, such as WeatherBench [41] and ERA5 [18]. Prevalent medium-range forecasting models (e.g., FourCastNet [27], GraphCast [28], and FengWu [6]) are commonly trained on the aforementioned hourly datasets to generate global forecasts with a time interval of 6-hour, can not offer finer predictions like 30-minute forecasts for nowcasting.

A **significant limitation** of current ML-based weather forecasting models [27, 2, 28, 6] lies in their black-box training paradigm [47, 14], that is, primarily focusing on learning the mapping of data pairs with a fixed lead time (e.g., 6 hours), without explicitly incorporating the laws of atmospheric dynamics which govern finer-grained physical evolution processes. Consequently, this training paradigm brings a significant challenge for weather forecasting: *existing black-box AI models are unable to generalize at finer temporal scales beyond the inherent time resolution of the training datasets due to the absence of fine-grained physics modeling.*

To address this challenge, we propose WeatherGFT, a physics-AI hybrid model capable of simulating weather changes on fine-grained time scales through a set of partial differential equations (PDEs) [44]. WeatherGFT consists of an encoder, multiple stacked **HybridBlocks** and a decoder. As the core of our model, HybridBlock contains two branches: One utilizes PDE kernels to conduct physical evolution over small time scales, while the other employs neural networks to learn unresolved atmospheric processes and perform bias correction on the physical evolution. These two branches are adaptively fused through a **learnable router** initialized as 0.5:0.5. Unlike existing models [27, 28, 6] trained with a fixed lead time, we introduce a **lead time-aware framework** through multi-lead time training strategy and a lead time conditional decoder, enabling the model to generalize to finer-grained temporal scales. Experiments demonstrate that our method is capable of forecasting at different lead times within one single model and one unified framework, overcoming the limitations of the dataset’s temporal resolution and *enabling 30-minute forecasts with an hourly dataset.*

Additionally, we find two interesting insights by examining the learnable route weight of the hybrid physical-AI modules at different lead times, as depicted in Figure 1: **a)** The physical weight is consistently higher than the AI, indicating the significant role played by the PDE kernel. **b)** As the lead time increases, the weight of AI gradually increases. We attribute this increment to the errors accumulation of PDE kernel during the evolution process, necessitating more AI corrections. In summary, when there is training data available at the lead time, such as at 1:00:00, the fitting ability of AI is enhanced. Conversely, at the lead time without training data, such as at 0:30:00, the importance of physical evolution becomes more pronounced, which confirms our motivation: **WeatherGFT can benefit from both physics and AI adaptively.**



Physical evolution time scale < Data time resolution
 Figure 1: **Learnable router weight.** The role of **physics** and **AI** at different lead times: **major evolution** and **adaptive correction** (details in Sec. 4.4).

We summarize the contributions of this paper as follows:

- We propose a physics-AI hybrid model that incorporates physical PDEs into the networks, enabling the simulation of fine-grained physical evolution through its forward process.
- With the flexible PDE kernel and new lead time-aware training framework, our model performs multiple lead time forecasts, which bridges the nowcast and medium-range forecast.
- For the first time, our model extends the forecasting ability learned from an hourly dataset to make accurate predictions at a finer time scale, i.e., 30 minutes.
- Our model achieves state-of-the-art (SOTA) performance in forecast tasks at different time scales, ranging from nowcast to medium-range forecast.

2 Related Work

Data-driven Weather Forecasting. In recent years, data-driven weather forecasting models based on machine learning have developed rapidly [1], especially for medium-range weather forecast [48], which provides weather variables for the next few days. Clare et al.[9] propose a weather forecasting approach using stacked ResNets [17], but their model only considers geopotential and temperature, which is limited for real-world forecasting applications. FourCastNet [27] expands the model to include additional variables such as wind at different heights, and employs Adaptive Fourier

Neural Operator (AFNO) [13] networks for prediction. Pangu-Weather [2] utilizes the 3D Swin Transformer [53] and introduces hierarchical temporal aggregation to minimize iterations in the autoregressive forecasting, followed by FengWu [6, 49], FuXi [7] and other Transformer-based [46] prediction models. Apart from Transformers, GraphCast [28] and Keisler [24] adopt a graph representation of the Earth and employ Graph Neural Network (GNN) [54] for weather prediction.

In addition to medium-range weather forecast, nowcast [3] is another important field in weather forecast, which usually provides 30-minute forecasting of severe convective weather like thunderstorms. OFAF [38], Preciplstm [36], SimVP [10] use convolutions to capture spatial information and model temporal information through networks such as Long Short-Term Memory [52] or Recurrent Neural Network [51]. Earthformer [11] and CasCast [12] use Transformer-based models for nowcasting. The former proposes cuboid attention to efficiently model space-time information, and the latter uses the diffusion model [43] to address the problem of blur output. These nowcast models focus on minute-level forecasts for specific regions, and is difficult to forecast for long-term such as 5-day.

Consequently, there exists a significant gap (global vs. regional, day-level vs. minute-level, long-term vs. short-term) between medium-range forecasts and nowcasts. Integrating AI models with physical guidance to make finer-grained predictions can bridge this gap.

Physical Neural Networks. Most data-driven models commonly neglect the incorporation of physics and treat networks as black-boxes. In order to enhance the consistency of predictions with respect to physical laws, PINNs [4], PINO [32], and DeepPhysiNet [30] add PDE loss to overall training loss. Nevertheless, these methods of changing loss functions often require balancing the weights between different PDEs, and the training results are heavily affected by hyperparameters. PIHC-MoE [5], ClimODE [47] integrate physical processes into the networks, but they do not explicitly simulate the physical evolution of distinct variables based on PDEs. Instead, they implement the evolution using general kernels, such as Euler kernels [45]. NeuralGCM [26] employs neural networks to parameterize a dynamic core. However, it is primarily designed for medium-range forecasting. These works typically focus on forecasting at fixed lead times, rather than leveraging physical laws to generalize to finer-grained time scales beyond the training datasets.

3 Method

3.1 Problem Formulation

Weather forecasting aims to predict future weather states \mathcal{X}_t given current weather states \mathcal{X}_0 :

$$F_\theta(\mathcal{X}_0) = P(\mathcal{X}_t|\mathcal{X}_0) \quad (1)$$

where θ represents the parameters of the model and t denotes the lead time. The weather state $\mathcal{X} \in \mathbb{R}^{C \times H \times W}$ consists of C atmospheric variables across different pressure levels. Each variable is characterized by an $H \times W$ matrix that corresponds to the projection of the Earth’s plane.

Assuming that the time resolution of the dataset is t_{data} , the lead time t for data-driven models can only be equal to or greater than t_{data} , because these models are trained using data pairs $(\mathcal{X}_0, \mathcal{X}_t)$ sampled from the dataset. Consequently, black-box AI models [27, 2, 28, 6, 16, 15] are unable to forecast at finer lead times such as $\frac{1}{2}t_{data}$, indicating a **lack of temporal generalization ability**.

3.2 WeatherGFT Overview

As shown in Figure 2, our model consists of an encoder to patchify the weather states into tokens [46], multiple (specifically, 24) stacked HybridBlocks to preform weather evolution via PDE modeling, and a decoder to generate predictions under specific lead-time conditions.

Specifically, to enable our model to generalize at a finer-grained temporal resolution, we employ PDEs to model the evolution at a finer time scale:

$$\mathcal{X}_{t_s} = \mathcal{K}(\mathcal{X}_0), \text{ where } t_s = \frac{1}{m}t_{data}, m \in \mathbb{Z}^+ \quad (2)$$

We simulate the physical evolution from \mathcal{X}_0 to \mathcal{X}_{t_s} through a uniquely designed PDE kernel (details in Section 3.3), where t_s is much smaller than the time resolution t_{data} of the dataset, allowing model to capture fine-grained weather changes. By stacking PDE kernels \mathcal{K} , the longer evolution can be achieved like $\mathcal{X}_{t_{data}} = \mathcal{K}_m \dots \mathcal{K}_2 \mathcal{K}_1 \mathcal{X}_0$. In this paper, we set m to 12, that is, $t_s = \frac{1}{12}t_{data}$.

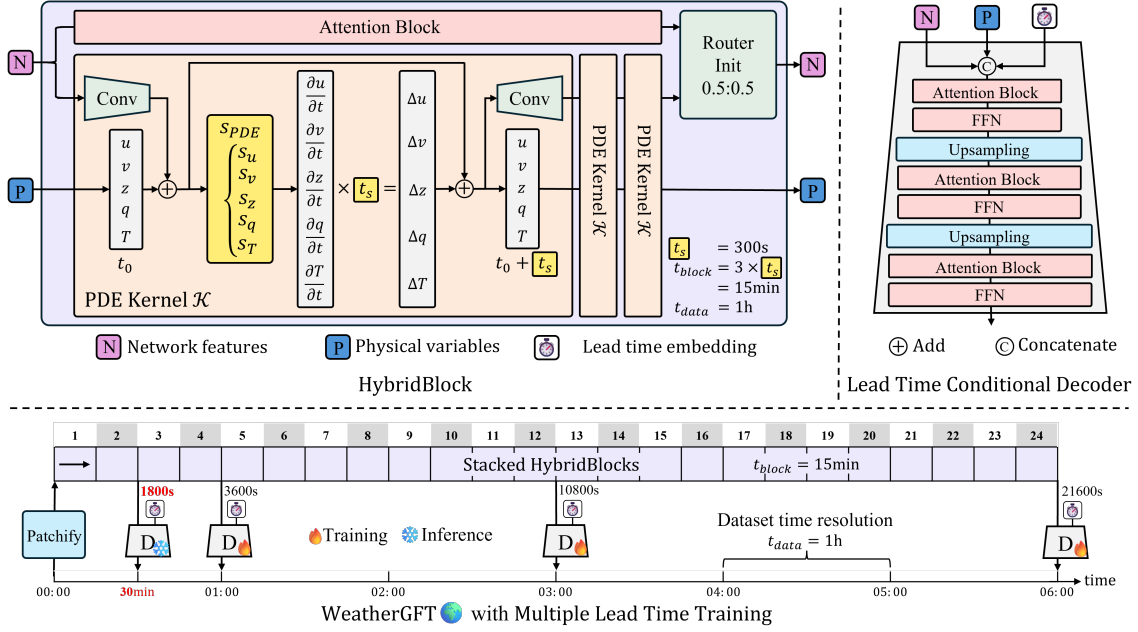


Figure 2: **Overview of WeatherGFT.** HybridBlock serves as the fundamental unit of the model, consisting of three PDE kernels, a parallel Attention Block, and a subsequent learnable router. A lead time conditional decoder is employed to generate forecasts for different lead times.

To mitigate the issue of error accumulation as the number of evolutionary steps increases, we introduce a parallel Attention Block [46] that performs bias correction for every 3 iterations of \mathcal{K} . Additionally, a learnable router initialized as 0.5 : 0.5, is employed to adaptively fuse features from PDE kernels and the Attention Block. We encapsulate three PDE kernels \mathcal{K} and one parallel Attention Block within a HybridBlock, whose evolution time is $t_{block} = 3 \times t_s = \frac{1}{4}t_{data}$.

Our model can not only forecast at lead times equal to or greater than t_{data} , but also generalize to finer-grained time scale such as $\frac{1}{2}t_{data}$ even in the absence of corresponding training data pairs. This is achieved by modeling the physical evolution of $t_{block} = \frac{1}{4}t_{data}$, rather than simply learning from data pairs $(\mathcal{X}_0, \mathcal{X}_{t_{data}})$ sampled from the dataset. Notably, these generalized finer-grained predictions of our model outperform temporal interpolation on multiple metrics, as shown in Table 3, emphasizing the advantages of fine-grained physical evolution over black-box models.

3.3 PDE Kernel

We employ a set of five PDEs (7-11) including the motion equation, the continuous equation and others to establish a closed system, which simulate the physical evolution of 5 essential atmospheric variables: u (latitude-direction wind), v (longitude-direction wind), z (geopotential), q (humidity), T (temperature). The partial derivative of each atmospheric variable with respect to time can be separated mathematically (details in Appendix A), denoted as S_{PDE} , which takes current weather state as input and produces the derivative of each variable with respect to time. We define PDE kernel \mathcal{K} as the evolution of the variables over a short period of time t_s , as demonstrated in Equation 3.

$$S_{PDE}(\mathcal{X}) = \begin{cases} \frac{\partial u}{\partial t} = S_u(u, v, z, q, T)16 \\ \frac{\partial v}{\partial t} = S_v(u, v, z, q, T)16 \\ \frac{\partial z}{\partial t} = S_z(u, v, z, q, T)21 \\ \frac{\partial q}{\partial t} = S_q(u, v, z, q, T)23 \\ \frac{\partial T}{\partial t} = S_T(u, v, z, q, T)18 \end{cases}, \quad \text{PDE Kernel } \mathcal{K}(\mathcal{X}) = S_{PDE}(\mathcal{X})t_s + \mathcal{X} \quad (3)$$

where $t_s = \frac{1}{12}t_{data}$

Calculating S_{PDE} requires the use of differential and integral operations. For example, for temperature T , its derivative with respect to time is shown in Equation 4. In order to efficiently calculate S_{PDE} and enable loss backward [20], we designed a fast implementation of differentiation and integration through convolution and matrix multiplication respectively. Equation 5 presents the implementation of the differential and integral of \mathcal{X} in the x direction (latitude direction).

$$\frac{\partial T}{\partial t} = \frac{-L \frac{\partial z}{\partial p} w - \frac{\partial z}{\partial p} w}{c_p} - u \frac{\partial T}{\partial x} - v \frac{\partial T}{\partial y} - w \frac{\partial T}{\partial p}, \text{ where } w = - \int \left(\frac{\partial u}{\partial x} + \frac{\partial v}{\partial y} \right) dp \quad (4)$$

$$\begin{cases} \frac{d\mathcal{X}}{dx} = \frac{1}{12} \text{Conv}(\mathcal{X}, K_x) \\ \int \mathcal{X} dx = \mathcal{X} M_x \end{cases}, K_x = \begin{bmatrix} 0 & 0 & 0 & 0 & 0 \\ 0 & 0 & 0 & 0 & 0 \\ 1 & -8 & 0 & 8 & -1 \\ 0 & 0 & 0 & 0 & 0 \\ 0 & 0 & 0 & 0 & 0 \end{bmatrix}, M_x = \begin{bmatrix} 1 & 1 & \dots & 1 & 1 \\ 0 & 1 & \dots & 1 & 1 \\ \vdots & \vdots & \ddots & \vdots & \vdots \\ 0 & 0 & \dots & 1 & 1 \\ 0 & 0 & \dots & 0 & 1 \end{bmatrix} \in \mathbb{R}^{W \times W} \quad (5)$$

Similarly, K_y and M_y can be constructed to perform differential and integral operations in the y direction (longitude direction). For differential and integral operations in the p direction (pressure level direction), we first reshape $\mathcal{X} \in \mathbb{R}^{C \times H \times W}$ to 3D space $\mathcal{X}_{3D} \in \mathbb{R}^{\frac{C}{P} \times P \times H \times W}$ based on the variables' pressure layers, and then implement corresponding operations through K_p and M_p .

3.4 HybridBlock with Adaptive Router

HybridBlock is a module that combines physics and AI. Firstly, it employs neural networks to address the issue of error accumulation resulting from the stacking of PDE kernel \mathcal{K} . Secondly, it utilizes the PDE kernel \mathcal{K} to guide the neural networks to learn the physical evolution of a specific time step. The structure of HybridBlock consists of three PDE kernels \mathcal{K} and one parallel Attention Block. Consequently, the time step corresponding to a HybridBlock is $t_{block} = 3 \times t_s = \frac{1}{4} t_{data}$.

HybridBlock has two branches, as depicted in Figure 2, one is physics and the other is AI. The neural networks features \mathcal{X}_N are aligned with physical features \mathcal{X}_P through a convolutional layer, followed by three PDE kernels. Subsequently, the PDE kernel output is projected back to the latent space of \mathcal{X}_N through another convolutional layer. Finally, features fusion is performed through the learnable router shown in Figure 3.

In the router, the features \mathcal{X}_N obtained from the neural networks and the features \mathcal{X}_P derived from the PDE kernels are initially linearly fused along the feature dimension D , with the learnable factor r initialized as 0.5 : 0.5. Subsequently, the preliminary fused features will go through an Multilayer Perceptron [35] layer containing a ReLU [31] activation function to accomplish nonlinear feature fusion.

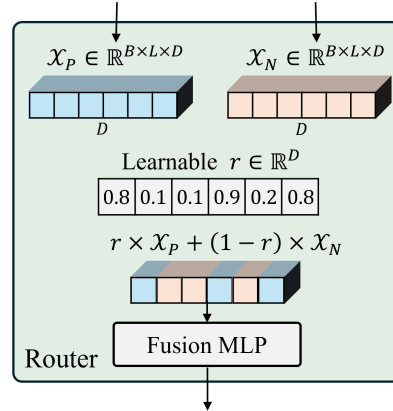


Figure 3: **Router in HybridBlock.** B represents batch size, L is the number of tokens with D dimension.

3.5 Lead Time Conditional Decoder

HybridBlock provides the smallest time scale of model evolution, which is $t_{block} = \frac{1}{4} t_{data}$. Through $L \times$ HybridBlocks, we can predict the weather at a lead time of $\frac{L}{4} t_{data}$. To enable the model to generalize its prediction capabilities to finer-grained time scales, we design a lead time conditional decoder to generate forecasts varying lead times from the output of the corresponding HybridBlock.

In order to promote the expression of the condition, we embed the lead time t into a high-dimensional vector t_{emb} through learnable Fourier embedding [42], as shown in Equation 6.

$$t_{emb} = \sin(\pi \cdot t \cdot W) \oplus \cos(\pi \cdot t \cdot W) \oplus t, \text{ where } t \text{ is lead time} \quad (6)$$

where W is a learnable vector of size 16, and \oplus denotes concatenation. Furthermore, t_{emb} will be concatenated with the output of HybridBlock and input to the decoder together. The decoder structure utilizes a Swin Transformer [34] with hierarchical upsampling, as illustrated in Figure 2.

3.6 Multiple Lead Time Training

For dataset like ERA5 [18] or WeatherBench [41], their time resolution is $t_{data} = 1\text{h}$. We set the time step of the PDE kernel to $t_s = \frac{1}{12} t_{data} = 300\text{s}$. Consequently, the time step of each HybridBlock is

$t_{block} = 3 \times t_s = 900s$, equivalent to 15 minutes. By cascading 24 HybridBlocks, model can generate forecasts at a lead time of $24 \times 15min = 6h$. To encourage the model to learn evolution for different lead times and generalize forecasting to finer-grained time scales, during training, we not only use the output of the last HybridBlock but also include the outputs of the 4th and 12th HybridBlocks. These outputs are passed through the lead time conditional decoder with corresponding t_{emb} to predict the weather states at $4 \times 15min = 1h$ and $12 \times 15min = 3h$.

During inference, we can take the output of the second HybridBlock and pass it through the decoder with corresponding t_{emb} to get $2 \times 15min = 30min$ forecasts, which are not present in the dataset. In the Section 4.3, we provide a comprehensive demonstration showcasing the accuracy of these generalized prediction results for time scales smaller than the dataset’s time resolution.

4 Experiment

Through the design of HybridBlock mixed with physics & AI and the multi-lead time training method, our model is capable of simultaneously conducting short-term forecasting and long-term forecasting without additional finetuning [37] on different forecasting tasks. In the experiments, we will showcase the superior performance of our model and try to answer the following questions:

- (1) How does the model perform on the medium-range forecasting task?
- (2) How does the model perform on the *generalized 30-minute nowcasting* task?
- (3) As a hybrid expert model of AI and physics, what roles do they each play?
- (4) How do PDE kernel and multi-lead time training contribute to the overall performance?

4.1 Experimental Setup

Dataset. We use WeatherBench [41] as our training dataset, whose time resolution is $t_{data} = 1h$ and spatial resolution is 128×256 . The dataset spanning from 1980 to 2015 serves as training set, while the data of 2017 is the validation and test sets. Our model processes 4 surface variables and 5 upper-air variables across 13 pressure levels, as shown in Table 2.

Given that WeatherBench lacks data at finer temporal resolutions, we use the 30-minute satellite observations downloaded from NASA as ground truth to quantitatively assess the model’s generalizability. NOTE: Data from NASA is only used for testing and not for model training.

Tasks. We conducted experiments on two typical weather forecasting tasks: medium-range forecasting and precipitation nowcasting. The forecast range for medium-range forecasting spans from 6 hours to 5 days, while the nowcasting is set to a range of 30 minutes to 2 hours.

Baseline Methods. We compare WeatherGFT with four forecast approaches: FourCastNet [27] uses AFNO [13] networks to simulate the nonlinear relationship between weather variables, Keisler [24] models global atmospheric data through GNN, ClimODE[47] adds ordinary differential equations (ODE) [21] to the neural networks, and ECMWF-IFS [40] is a physical dynamic model.

The above three data-driven models cannot generalize forecasting to finer-grained time scales due to the absence of 30-minute labels. Therefore, in nowcasting tasks, we interpolate the 30-minute forecast results through SOTA frame interpolation models Flavr [23] and UPR [22]. In contrast, our model can conduct 30-minute predictions inherently without interpolating.

Implementation Details. We implemented the model with PyTorch [20] and trained 50 epochs on 8 NVIDIA A100 GPUs [8] for 3 days, with a learning rate of cosine schedule starting from $5e-4$.

Dataset	Train	Test	Time resolution
WeatherBench	✓	✓	1-hour
NASA	×	✓	30-minute

Table 1: **Datasets.** NASA dataset only contains precipitation, which will be used as the ground truth for precipitation nowcast.

Name	Description	Levels
u10	x-direction wind at 10m height	Single
v10	y-direction wind at 10m height	Single
t2m	Temperature at 2m height	Single
tp	Hourly precipitation	Single
z	Geopotential	13
q	Specific humidity	13
u	x-direction wind	13
v	y-direction wind	13
T	Temperature	13

Table 2: **Atmospheric Variables Considered.** The 13 levels are 50, 100, 150, 200, 250, 300, 400, 500, 600, 700, 850, 925, 1000 hPa.

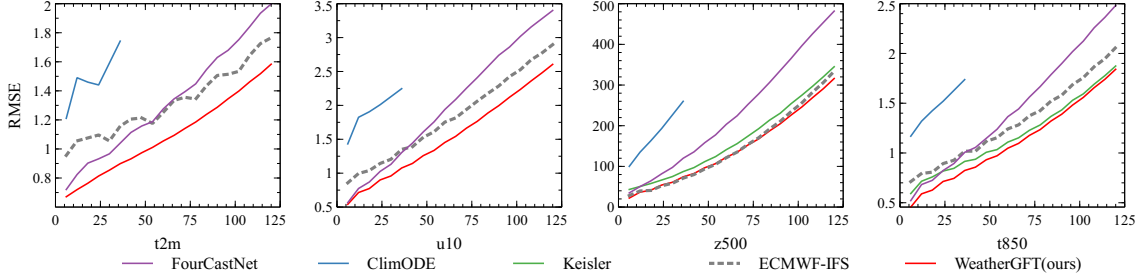


Figure 4: **Medium-Range Forecast.** The x-axis represents the lead time in hours, while the y-axis represents the RMSE for different variables. The smaller RMSE the better.

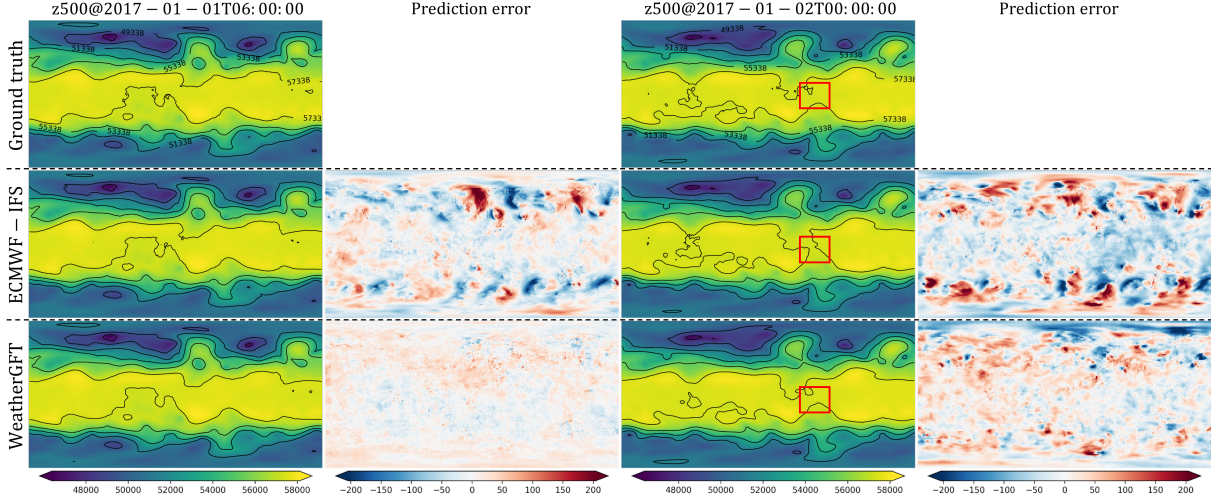


Figure 5: **Visualization of z500 Predictions.**

4.2 Skillful Medium-Range Forecasts by WeatherGFT

Autoregression is commonly employed in medium-term forecasting, where the model output serves as the input for the subsequent forecast step, allowing for longer lead time predictions. However, prediction errors tend to accumulate during the autoregression, leading to an increase in the root mean square error (RMSE). As a result, a smaller RMSE indicates a more accurate prediction.

Figure 4 illustrates the changes in prediction RMSE of different weather variables as lead time increases. Our model demonstrates SOTA performance across various lead times, especially the prediction of surface temperature (t2m) and surface wind speed (u10) is significantly better than other models. The geopotential of the 500hpa pressure layer (z500) is a crucial weather variable in weather forecasting, as it reflects atmospheric circulation [39], subtropical high-pressure systems [29], and other significant phenomena. Due to the modeling of geopotential in the PDE 21, z500 prediction of our model outperforms the physical dynamic model ECMWF-IFS as visualized in Figure 5.

From the visualization in Figure 5, our model is more accurate in predicting the subtropical high, as indicated by the highlighted red box. In addition, the prediction error of our model at the lead time of 6-hour is significantly smaller than that of the physical dynamic model ECMWF-IFS.

4.3 Generalizing to Fine-grained Time Scale for Nowcasting

In contrast to conventional black-box AI models [27, 24, 50] used in medium-range weather forecasting, WeatherGFT has the ability to break through the time scale limitations of the dataset, making the generalization to fine-grained temporal scales possible. This capability is facilitated by the dynamic progression of our PDE kernel modeling and multiple lead time training. Specifically, we use the second HybridBlock of the total 24 HybridBlocks to generate 30-minute generalized forecasts through the lead time conditional decoder, which is very important for precipitation nowcasting.

To quantify the accuracy of the model’s generalized nowcasting, we utilize the NASA satellite precipitation observation dataset as the ground truth, which has a time resolution of 30-minute. We

	30-min			60-min			90-min			120-min		
	CSI \uparrow @0.5	CSI \uparrow @1.5	RMSE \downarrow tp1h	CSI \uparrow @0.5	CSI \uparrow @1.5	RMSE \downarrow tp1h	CSI \uparrow @0.5	CSI \uparrow @1.5	RMSE \downarrow tp1h	CSI \uparrow @0.5	CSI \uparrow @1.5	RMSE \downarrow tp1h
FourCast+Flavr	0.26	0.09	0.67	0.61	0.49	0.24	0.25	0.09	0.65	0.37	0.26	0.46
FourCast+UPR	0.20	0.10	0.76	0.61	0.49	0.24	0.11	0.05	1.49	0.37	0.26	0.46
Keisler+Flavr	0.25	0.09	0.66	0.59	0.48	0.23	0.25	0.08	0.66	0.41	0.29	0.35
Keisler+UPR	0.26	0.13	0.69	0.59	0.48	0.23	0.26	0.13	0.68	0.41	0.29	0.35
ClimODE+Flavr	0.26	0.09	0.67	0.62	0.51	0.22	0.25	0.09	0.66	0.47	0.34	0.32
ClimODE+UPR	0.25	0.12	0.67	0.62	0.49	0.21	0.25	0.11	0.66	0.46	0.32	0.31
WeatherGFT(ours)	0.28	0.17	0.72	0.62	0.50	0.21	0.28	0.16	0.71	0.54	0.40	0.27

Table 3: **Generalized Nowcast.** 60-min and 120-min are trained lead times, while 30-min and 90-min are generalized lead times. **Gray** represents the results obtained through the frame interpolation model, **purple** indicates the results obtained through our unified model without interpolating. For precipitation nowcasting, CSI (Critical Success Index) is the most important metric.

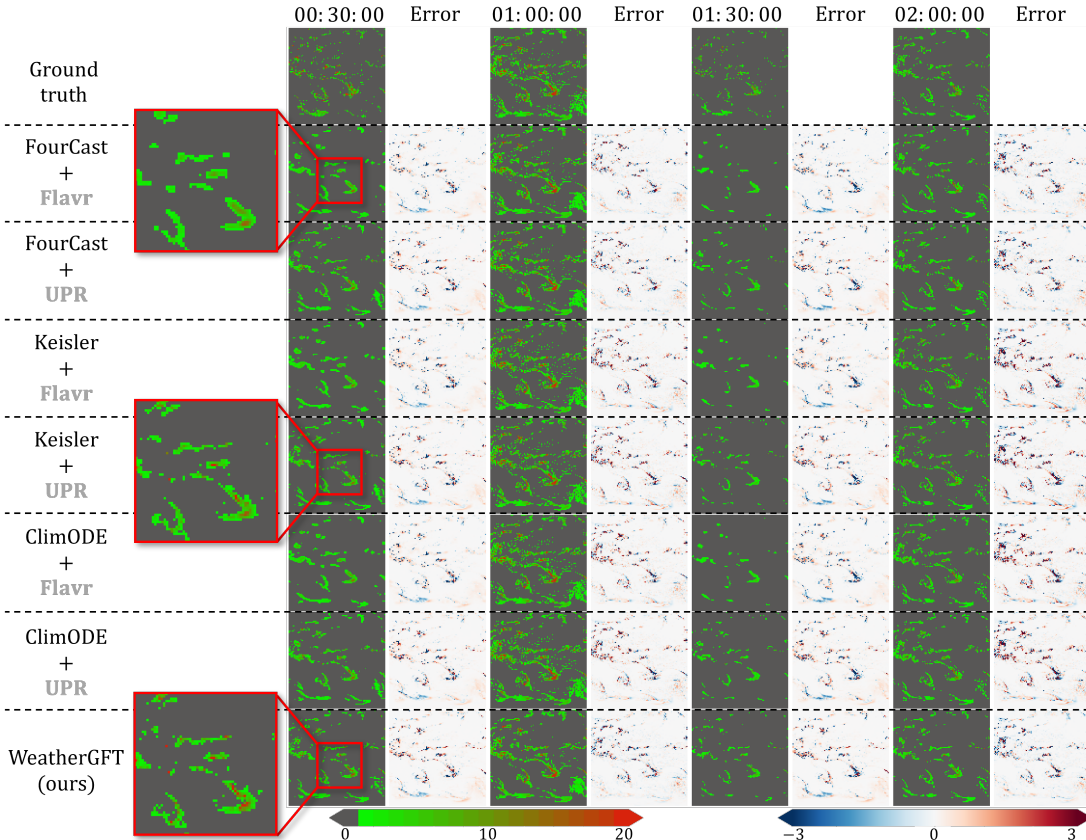


Figure 6: **Visualization of Precipitation Nowcast.** Precipitation in the area ranging from 34°N to 50°S and 148°E to 128°W during the time period from 00:00 to 02:00 on July 1, 2017.

evaluate forecasts at 30, 60, 90, and 120 minutes. It is important to note that data of NASA were not used for training. For other comparison models that cannot directly produce half-hour forecasts, we use the frame interpolation models (i.e., Flavr [23] and UPR [22]) to generate 30-minute predictions.

CSI@th (Critical Success Index) refers to the hit rate of the area that reaches the threshold precipitation value th. CSI@0.5 can reflect the overall forecast accuracy in rainy areas, and CSI@1.5 reflects the forecast accuracy in moderate rainy areas. Table 3 shows that our model surpasses others across different lead times, especially in forecasting regions of moderate rainfall, i.e., CSI@1.5.

The visualization in Figure 6 reveals that when using frame interpolation to obtain 30-minute predictions, there is blurring occurring at different scales, resulting in the loss of extreme values, as indicated in the red box. Our model, which incorporates physical constraints, provides clearer predictions retaining extreme values without the need for frame interpolation.

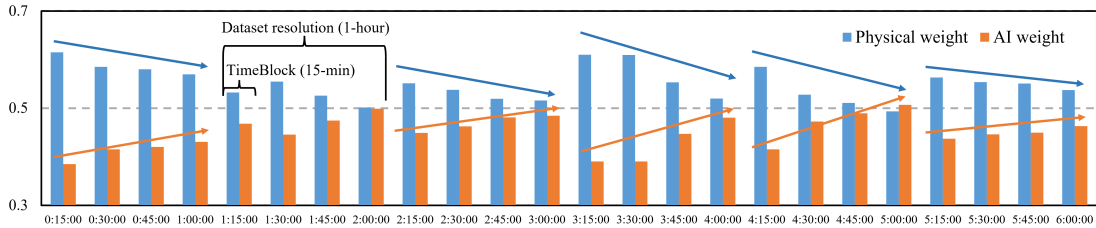


Figure 7: The Weights in the Router of 24 HybridBlocks.

4.4 Weather Forecasts can Benefit from Physics and AI via WeatherGFT

As a hybrid model combining both physics and AI components, it is crucial to analyze their contributions to the prediction process. We present insights into their respective proportions by visualizing the weight parameter r within the learnable router (refer to Figure 3). The visualization in Figure 7 reveals that the weights of the 24 HybridBlocks display a similar distribution:

a) The physical weight of the vast majority of HybridBlocks is significantly higher than the weight of AI, which shows that in the process of simulating time evolution, the PDE kernel plays a more important role, while the Attention Block only plays a supportive correction role. **b)** The physical weight gradually decreases while the weight of AI increases throughout each hour (dataset time resolution). This aligns with our underlying motivation, which acknowledges that errors may accumulate over time in the physics-based evolution. Consequently, a greater emphasis on AI corrections becomes necessary to compensate for these accumulated errors.

By averaging the 4×6 HybridBlocks into 4 time steps, the average weight every 15-minute is obtained in Figure 1, which shows the above two conclusions more clearly. To summarize, physics plays the main evolutionary role in the model, while AI plays an dynamic corrective role.

4.5 Ablation Studies

We use Swin Attention Block [34] as the baseline for the ablation studies. For this baseline networks without PDE kernel constraints, as a black-box model, it will only learn the mapping of data pairs corresponding to the lead time. Consequently, its internal information between blocks is unexplainable, which also results in being unable to predict moments without data labels, such as 30-minute nowcasting.

PDE kernel is crucial to the generalization of finer-grained predictions. Instead of simply learning the mapping between data, the model learns the evolution of the corresponding time step according to the physics laws, making information of each neural network layer explainable, thereby facilitating generalized 30-minute nowcasting. In addition, we find that the introduction of the PDE kernel also improved the prediction accuracy of the model.

Multiple lead time training accelerates convergence and improves the accuracy of model prediction, as shown in Figure 8. We hypothesize that this phenomenon can be attributed to the loss backward from different lead times, which alleviates the issue of vanishing gradients [19], allowing the parameters of different layers to quickly warm up and improve the expression of the model.

5 Conclusion

Most existing data-driven weather forecast methods which operated as black-box models via purely performing data mapping are unable to generalize at finer temporal scale beyond the inherent time

	30-min nowcast	RMSE@1-h t2m↓ z500↓	RMSE@6-h t2m↓ z500↓	RMSE@3-d t2m↓ z500↓
Attent Block	×	0.52 18.76	0.73 24.21	1.23 157.9
+ PDE Kernel	✓	0.57 20.43	0.70 21.78	1.22 153.8
+ Muti Time	✓	0.49 16.66	0.67 21.80	1.14 152.4

Table 4: Ablation Experiment.

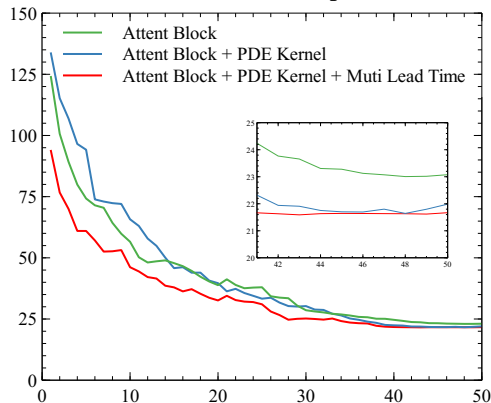


Figure 8: RMSE z500 as Training Epochs.

resolution of the training datasets due to the absence of the fine-grained physics modeling. This paper proposes a physics-AI hybrid model to solve this problem. Through the exquisitely designed PDE kernel, each block in the networks can simulate the evolution of physical variables at finer-gained time step, while AI plays the role of adaptive correction, which makes our model capable of generalizing predictions to a finer time scale beyond dataset. By employing our proposed multi-lead time training strategy, our model trained on an hourly dataset exhibits remarkable ability of generalized 30-minute forecasts, achieving SOTA performance in both medium-range forecast and precipitation nowcast.

The limitation of our model lies in the relatively small number of PDEs incorporated in our method. For future work, we will augment WeatherGFT with more physical laws, as indicated in Appendix C.

References

- [1] Zied Ben Bouallègue, Mariana CA Clare, Linus Magnusson, Estibaliz Gascon, Michael Maier-Gerber, Martin Janoušek, Mark Rodwell, Florian Pinault, Jesper S Dramsch, Simon TK Lang, et al. The rise of data-driven weather forecasting: A first statistical assessment of machine learning-based weather forecasts in an operational-like context. *Bulletin of the American Meteorological Society*, 2024.
- [2] Kaifeng Bi, Lingxi Xie, Hengheng Zhang, Xin Chen, Xiaotao Gu, and Qi Tian. Accurate medium-range global weather forecasting with 3d neural networks. *Nature*, 619(7970):533–538, 2023.
- [3] KA Browning and CiG Collier. Nowcasting of precipitation systems. *Reviews of Geophysics*, 27(3):345–370, 1989.
- [4] Shengze Cai, Zhiping Mao, Zhicheng Wang, Minglang Yin, and George Em Karniadakis. Physics-informed neural networks (pinns) for fluid mechanics: A review. *Acta Mechanica Sinica*, 37(12):1727–1738, 2021.
- [5] Nithin Chalapathi, Yiheng Du, and Aditi Krishnapriyan. Scaling physics-informed hard constraints with mixture-of-experts. *arXiv preprint arXiv:2402.13412*, 2024.
- [6] Kang Chen, Tao Han, Junchao Gong, Lei Bai, Fenghua Ling, Jing-Jia Luo, Xi Chen, Leiming Ma, Tianning Zhang, Rui Su, et al. Fengwu: Pushing the skillful global medium-range weather forecast beyond 10 days lead. *arXiv preprint arXiv:2304.02948*, 2023.
- [7] Lei Chen, Xiaohui Zhong, Feng Zhang, Yuan Cheng, Yinghui Xu, Yuan Qi, and Hao Li. Fuxi: a cascade machine learning forecasting system for 15-day global weather forecast. *npj Climate and Atmospheric Science*, 6(1):190, 2023.
- [8] Jack Choquette and Wish Gandhi. Nvidia a100 gpu: Performance & innovation for gpu computing. In *2020 IEEE Hot Chips 32 Symposium (HCS)*, pages 1–43. IEEE Computer Society, 2020.
- [9] Mariana CA Clare, Omar Jamil, and Cyril J Morcrette. Combining distribution-based neural networks to predict weather forecast probabilities. *Quarterly Journal of the Royal Meteorological Society*, 147(741):4337–4357, 2021.
- [10] Zhangyang Gao, Cheng Tan, Lirong Wu, and Stan Z Li. Simvp: Simpler yet better video prediction. In *Proceedings of the IEEE/CVF conference on computer vision and pattern recognition*, pages 3170–3180, 2022.
- [11] Zhihan Gao, Xingjian Shi, Hao Wang, Yi Zhu, Yuyang Bernie Wang, Mu Li, and Dit-Yan Yeung. Earthformer: Exploring space-time transformers for earth system forecasting. *Advances in Neural Information Processing Systems*, 35:25390–25403, 2022.
- [12] Junchao Gong, Lei Bai, Peng Ye, Wanghan Xu, Na Liu, Jianhua Dai, Xiaokang Yang, and Wanli Ouyang. Cascast: Skillful high-resolution precipitation nowcasting via cascaded modelling. *arXiv preprint arXiv:2402.04290*, 2024.
- [13] John Guibas, Morteza Mardani, Zongyi Li, Andrew Tao, Anima Anandkumar, and Bryan Catanzaro. Adaptive fourier neural operators: Efficient token mixers for transformers. *arXiv preprint arXiv:2111.13587*, 2021.
- [14] Riccardo Guidotti, Anna Monreale, Salvatore Ruggieri, Franco Turini, Fosca Giannotti, and Dino Pedreschi. A survey of methods for explaining black box models. *ACM computing surveys (CSUR)*, 51(5):1–42, 2018.
- [15] Tao Han, Song Guo, Fenghua Ling, Kang Chen, Junchao Gong, Jingjia Luo, Junxia Gu, Kan Dai, Wanli Ouyang, and Lei Bai. Fengwu-ghr: Learning the kilometer-scale medium-range global weather forecasting. *arXiv preprint arXiv:2402.00059*, 2024.
- [16] Tao Han, Song Guo, Wanghan Xu, Lei Bai, et al. Cra5: Extreme compression of era5 for portable global climate and weather research via an efficient variational transformer. *arXiv preprint arXiv:2405.03376*, 2024.

- [17] Kaiming He, Xiangyu Zhang, Shaoqing Ren, and Jian Sun. Deep residual learning for image recognition. In *Proceedings of the IEEE conference on computer vision and pattern recognition*, pages 770–778, 2016.
- [18] Hans Hersbach, Bill Bell, Paul Berrisford, Shoji Hirahara, András Horányi, Joaquín Muñoz-Sabater, Julien Nicolas, Carole Peubey, Raluca Radu, Dinand Schepers, et al. The era5 global reanalysis. *Quarterly Journal of the Royal Meteorological Society*, 146(730):1999–2049, 2020.
- [19] Sepp Hochreiter. The vanishing gradient problem during learning recurrent neural nets and problem solutions. *International Journal of Uncertainty, Fuzziness and Knowledge-Based Systems*, 6(02):107–116, 1998.
- [20] Sagar Imambi, Kolla Bhanu Prakash, and GR Kanagachidambaresan. Pytorch. *Programming with TensorFlow: Solution for Edge Computing Applications*, pages 87–104, 2021.
- [21] Edward L Ince. *Ordinary differential equations*. Courier Corporation, 1956.
- [22] Xin Jin, Longhai Wu, Jie Chen, Youxin Chen, Jayoon Koo, and Cheul-hee Hahm. A unified pyramid recurrent network for video frame interpolation. In *Proceedings of the IEEE/CVF Conference on Computer Vision and Pattern Recognition*, pages 1578–1587, 2023.
- [23] Tarun Kalluri, Deepak Pathak, Manmohan Chandraker, and Du Tran. Flavr: Flow-agnostic video representations for fast frame interpolation. In *Proceedings of the IEEE/CVF winter conference on applications of computer vision*, pages 2071–2082, 2023.
- [24] Ryan Keisler. Forecasting global weather with graph neural networks. *arXiv preprint arXiv:2202.07575*, 2022.
- [25] Ryuji Kimura. Numerical weather prediction. *Journal of Wind Engineering and Industrial Aerodynamics*, 90(12-15):1403–1414, 2002.
- [26] Dmitrii Kochkov, Janni Yuval, Ian Langmore, Peter Norgaard, Jamie Smith, Griffin Mooers, James Lottes, Stephan Rasp, Peter Düben, Milan Klöwer, et al. Neural general circulation models. *arXiv preprint arXiv:2311.07222*, 2023.
- [27] Thorsten Kurth, Shashank Subramanian, Peter Harrington, Jaideep Pathak, Morteza Mardani, David Hall, Andrea Miele, Karthik Kashinath, and Anima Anandkumar. Fourcastnet: Accelerating global high-resolution weather forecasting using adaptive fourier neural operators. In *Proceedings of the platform for advanced scientific computing conference*, pages 1–11, 2023.
- [28] Remi Lam, Alvaro Sanchez-Gonzalez, Matthew Willson, Peter Wirnsberger, Meire Fortunato, Ferran Alet, Suman Ravuri, Timo Ewalds, Zach Eaton-Rosen, Weihua Hu, et al. Learning skillful medium-range global weather forecasting. *Science*, 382(6677):1416–1421, 2023.
- [29] Hassan Lashkari and Zeinab Mohammadi. Study on the role of annual movements of arabian subtropical high pressure in the late start of precipitation in southern and southwestern iran. *Theoretical and applied climatology*, 137:2069–2076, 2019.
- [30] Wenyuan Li, Zili Liu, Keyan Chen, Hao Chen, Shunlin Liang, Zhengxia Zou, and Zhenwei Shi. Deepphysinet: Bridging deep learning and atmospheric physics for accurate and continuous weather modeling. *arXiv preprint arXiv:2401.04125*, 2024.
- [31] Yuanzhi Li and Yang Yuan. Convergence analysis of two-layer neural networks with relu activation. *Advances in neural information processing systems*, 30, 2017.
- [32] Zongyi Li, Hongkai Zheng, Nikola Kovachki, David Jin, Haoxuan Chen, Burigede Liu, Kamyar Azizzadenesheli, and Anima Anandkumar. Physics-informed neural operator for learning partial differential equations. *ACM/JMS Journal of Data Science*, 2021.
- [33] Fenghua Ling, Lin Ouyang, Boufeniza Redouane Larbi, Jing-Jia Luo, Tao Han, Xiaohui Zhong, and Lei Bai. Is artificial intelligence providing the second revolution for weather forecasting? *arXiv preprint arXiv:2401.16669*, 2024.

- [34] Ze Liu, Yutong Lin, Yue Cao, Han Hu, Yixuan Wei, Zheng Zhang, Stephen Lin, and Baining Guo. Swin transformer: Hierarchical vision transformer using shifted windows. In *Proceedings of the IEEE/CVF international conference on computer vision*, pages 10012–10022, 2021.
- [35] Ian D Longstaff and John F Cross. A pattern recognition approach to understanding the multi-layer perception. *Pattern Recognition Letters*, 5(5):315–319, 1987.
- [36] Zhifeng Ma, Hao Zhang, and Jie Liu. Preciplstm: A meteorological spatiotemporal lstm for precipitation nowcasting. *IEEE Transactions on Geoscience and Remote Sensing*, 60:1–8, 2022.
- [37] Julieta Martinez, Jashan Shewakramani, Ting Wei Liu, Ioan Andrei Bârsan, Wenyuan Zeng, and Raquel Urtasun. Permute, quantize, and fine-tune: Efficient compression of neural networks. In *Proceedings of the IEEE/CVF conference on computer vision and pattern recognition*, pages 15699–15708, 2021.
- [38] Tengfei Nie, Xiang Ji, and YuYing Pang. Ofaf-convlstm: an optical flow attention fusion-convlstm model for precipitation nowcasting. In *2021 3rd International Academic Exchange Conference on Science and Technology Innovation (IAECST)*, pages 283–286. IEEE, 2021.
- [39] Abraham H Oort and Eugene M Rasmusson. *Atmospheric circulation statistics*, volume 5. US Department of Commerce, National Oceanic and Atmospheric Administration . . . , 1971.
- [40] Anders Persson and Federico Grazzini. User guide to ecmwf forecast products. *Meteorological Bulletin*, 3(2), 2007.
- [41] Stephan Rasp, Peter D Dueben, Sebastian Scher, Jonathan A Weyn, Soukayna Mouatadid, and Nils Thuerey. Weatherbench: a benchmark data set for data-driven weather forecasting. *Journal of Advances in Modeling Earth Systems*, 12(11):e2020MS002203, 2020.
- [42] Tim Salimans and Jonathan Ho. Progressive distillation for fast sampling of diffusion models. *arXiv preprint arXiv:2202.00512*, 2022.
- [43] Jiaming Song, Chenlin Meng, and Stefano Ermon. Denoising diffusion implicit models. *arXiv preprint arXiv:2010.02502*, 2020.
- [44] Walter A Strauss. *Partial differential equations: An introduction*. John Wiley & Sons, 2007.
- [45] Shashank Reddy Vadyala, Sai Nethra Betgeri, and Naga Parameshwari Betgeri. Physics-informed neural network method for solving one-dimensional advection equation using pytorch. *Array*, 13:100110, 2022.
- [46] Ashish Vaswani, Noam Shazeer, Niki Parmar, Jakob Uszkoreit, Llion Jones, Aidan N Gomez, Łukasz Kaiser, and Illia Polosukhin. Attention is all you need. *Advances in neural information processing systems*, 30, 2017.
- [47] Yogesh Verma, Markus Heinonen, and Vikas Garg. Climode: Climate and weather forecasting with physics-informed neural odes. *arXiv preprint arXiv:2404.10024*, 2024.
- [48] A James Wagner. Medium-and long-range forecasting. *Weather and Forecasting*, 4(3):413–426, 1989.
- [49] Yi Xiao, Lei Bai, Wei Xue, Kang Chen, Tao Han, and Wanli Ouyang. Fengwu-4dvar: Coupling the data-driven weather forecasting model with 4d variational assimilation. *arXiv preprint arXiv:2312.12455*, 2023.
- [50] Wanghan Xu, Kang Chen, Tao Han, Hao Chen, Wanli Ouyang, and Lei Bai. Extremecast: Boosting extreme value prediction for global weather forecast. *arXiv preprint arXiv:2402.01295*, 2024.
- [51] Wenpeng Yin, Katharina Kann, Mo Yu, and Hinrich Schütze. Comparative study of cnn and rnn for natural language processing. *arXiv preprint arXiv:1702.01923*, 2017.
- [52] Yong Yu, Xiaosheng Si, Changhua Hu, and Jianxun Zhang. A review of recurrent neural networks: Lstm cells and network architectures. *Neural computation*, 31(7):1235–1270, 2019.

- [53] Yonghong Zhang, Xuquan Ji, Wenyong Liu, Zhuofu Li, Jian Zhang, Shanshan Liu, Woquan Zhong, Lei Hu, Weishi Li, et al. A spine segmentation method under an arbitrary field of view based on 3d swin transformer. *International Journal of Intelligent Systems*, 2023, 2023.
- [54] Jie Zhou, Ganqu Cui, Shengding Hu, Zhengyan Zhang, Cheng Yang, Zhiyuan Liu, Lifeng Wang, Changcheng Li, and Maosong Sun. Graph neural networks: A review of methods and applications. *AI open*, 1:57–81, 2020.

A PDE Solver

We constrain 5 atmospheric variables, that is, u (latitude-direction wind), v (longitude-direction wind), z or ϕ (geopotential), q (humidity), T (temperature), through the following set of five partial differential equations (PDEs) [25]:

$$\frac{d\mathbf{V}}{dt} + f\mathbf{k} \times \mathbf{V} = -g\nabla_p z + \mathbf{F}_h \quad (7)$$

$$\frac{\partial\phi}{\partial p} = -\frac{1}{\rho} \quad (8)$$

$$\nabla_p \cdot \mathbf{V} + \frac{\partial w}{\partial p} = 0 \quad (9)$$

$$c_p \frac{dT}{dt} - \frac{1}{\rho} w = Q \quad (10)$$

$$p = \rho RT \quad (11)$$

The expansion of $\frac{d}{dt}$ is as follows:

$$\frac{d}{dt} = \left(\frac{\partial}{\partial t} \right)_p + \mathbf{V} \cdot \nabla_p (\) + w \frac{\partial}{\partial p} \quad (12)$$

The PDE above is in the pressure coordinate system, which is aligned with the input to our model, as the input to the model comes from 13 pressure layers. In the air pressure coordinate system, the following equation is also satisfied:

$$\frac{\partial p}{\partial t} = 0 \quad (13)$$

w represents the vertical wind speed and is not directly included as one of the input variables in our model. However, it can be derived from u and v using following equation:

$$\begin{aligned} \frac{\partial w}{\partial p} &= -\frac{\partial u}{\partial x} - \frac{\partial v}{\partial y} \\ w &= -\int \left(\frac{\partial u}{\partial x} + \frac{\partial v}{\partial y} \right) dp \end{aligned} \quad (14)$$

After getting w , we can get $\frac{\partial u}{\partial t}$ and $\frac{\partial v}{\partial t}$ according to Equation 7.

$$\begin{cases} \frac{\partial u}{\partial t} + u \frac{\partial u}{\partial x} + v \frac{\partial u}{\partial y} + w \frac{\partial u}{\partial p} - fv = -\frac{\partial\phi}{\partial x} \\ \frac{\partial v}{\partial t} + u \frac{\partial v}{\partial x} + v \frac{\partial v}{\partial y} + w \frac{\partial v}{\partial p} + fu = -\frac{\partial\phi}{\partial y} \end{cases} \quad (15)$$

$$\begin{cases} \frac{\partial u}{\partial t} = -u \frac{\partial u}{\partial x} - v \frac{\partial u}{\partial y} - w \frac{\partial u}{\partial p} + fv - \frac{\partial\phi}{\partial x} \\ \frac{\partial v}{\partial t} = -u \frac{\partial v}{\partial x} - v \frac{\partial v}{\partial y} - w \frac{\partial v}{\partial p} - fu - \frac{\partial\phi}{\partial y} \end{cases} \quad (16)$$

where $f = 7.29e - 5$ is a constant.

According to Equation 10, we can get $\frac{\partial T}{\partial t}$:

$$\begin{cases} c_p \left(\frac{\partial T}{\partial t} + u \frac{\partial T}{\partial x} + v \frac{\partial T}{\partial y} + w \frac{\partial T}{\partial p} \right) - \frac{1}{\rho} w = Q \\ Q = -L \frac{\partial \phi}{\partial p} w \end{cases} \quad (17)$$

$$\frac{\partial T}{\partial t} = \frac{-L \frac{\partial \phi}{\partial p} w - \frac{\partial \phi}{\partial p} w}{c_p} - u \frac{\partial T}{\partial x} - v \frac{\partial T}{\partial y} - w \frac{\partial T}{\partial p} \quad (18)$$

where $L = 2.5e6$ and $c_p = 1005$ are constants.

According to Equations 8 and Equations 11, we can get $\frac{\partial \phi}{\partial t}$:

$$\frac{\partial \phi}{\partial p} = -\frac{1}{\rho} = -\frac{RT}{p} \quad (19)$$

$$\begin{aligned} \frac{\partial^2 \phi}{\partial p \partial t} &= -\frac{\partial \frac{RT}{p}}{\partial t} \\ &= -R \left(\frac{1}{p} \frac{\partial T}{\partial t} - \frac{T}{p^2} \frac{\partial p}{\partial t} \right) \\ &= -\frac{R}{p} \frac{\partial T}{\partial t} \end{aligned} \quad (20)$$

$$\begin{aligned} \frac{\partial \phi}{\partial t} &= \int \frac{\partial^2 \phi}{\partial p \partial t} dp \\ &= -\int \frac{R}{p} \frac{\partial T}{\partial t} dp \end{aligned} \quad (21)$$

where $R = 8.314$ is a constant.

Finally, according to the water vapor equation 22, we can get $\frac{\partial q}{\partial t}$:

$$\begin{cases} \frac{dq}{dt} = \frac{\delta F}{RT} \frac{d\phi}{dt} \\ \delta = \begin{cases} 0, & \frac{d\phi}{dt} < 0 \text{ and } q \geq q_s \\ 1, & \text{else} \end{cases} \\ F = q_s T \frac{LR - c_p R_v T}{c_p R_v T^2 + L^2 q_s} \\ e_s = 6.112 \times \exp \left(\frac{17.67 T'}{T' + 243.5} \right) \\ T' = T - 273.15 \\ q_s = \frac{0.622 e_s}{p - 0.378 e_s} \end{cases} \quad (22)$$

$$\frac{\partial q}{\partial t} = \frac{\delta F}{RT} \left(\frac{\partial \phi}{\partial t} + u \frac{\partial \phi}{\partial x} + v \frac{\partial \phi}{\partial y} + w \frac{\partial \phi}{\partial z} \right) - u \frac{\partial q}{\partial x} - v \frac{\partial q}{\partial y} - w \frac{\partial q}{\partial z} \quad (23)$$

where $R_v = 461.5$ and $R_d = 287$ are constants.

B Implementation of Integrals and Differentials

Integral in p-direction (pressure levels direction) is implemented with PyTorch [20] as follows:

```
def integral_z(input_tensor):
    B, C, H, W = input_tensor.shape
    input_tensor = input_tensor.reshape(B, C, H*W)
    output = integral_mask.to(input_tensor.dtype).to(input_tensor.
                                                    device) @ input_tensor
    output = output.reshape(B, C, H, W)
    return output
```

Differentials in x-direction (latitude direction) is implemented with PyTorch as follows:

```
def d_x(input_tensor):
    B, C, H, W = input_tensor.shape
    conv_kernel = torch.zeros([1,1,1,5], device=input_tensor.device,
                              dtype=input_tensor.dtype,
                              requires_grad=False)

    conv_kernel[0,0,0,0] = 1
    conv_kernel[0,0,0,1] = -8
    conv_kernel[0,0,0,3] = 8
    conv_kernel[0,0,0,4] = -1

    input_tensor = torch.cat((input_tensor[:, :, :, -2:],
                              input_tensor,
                              input_tensor[:, :, :, :2]), dim=3)
    _, _, H_, W_ = input_tensor.shape

    input_tensor = input_tensor.reshape(B*C, 1, H_, W_)
    output_x = F.conv2d(input_tensor, conv_kernel)/12
    output_x = output_x.reshape(B, C, H, W)
    output_x = output_x/pixel_x.to(output_x.dtype).to(output_x.device)

    return output_x
```

Differentials in y-direction (longitude direction) is implemented with PyTorch as follows:

```
def d_y(input_tensor):
    B, C, H, W = input_tensor.shape
    conv_kernel = torch.zeros([1,1,5,1], device=input_tensor.device,
                              dtype=input_tensor.dtype,
                              requires_grad=False)

    conv_kernel[0,0,0] = -1
    conv_kernel[0,0,1] = 8
    conv_kernel[0,0,3] = -8
    conv_kernel[0,0,4] = 1

    input_tensor = torch.cat((input_tensor[:, :, :2],
                              input_tensor,
                              input_tensor[:, :, -2:]), dim=2)
    _, _, H_, W_ = input_tensor.shape

    input_tensor = input_tensor.reshape(B*C, 1, H_, W_)
    output_y = F.conv2d(input_tensor, conv_kernel)/12
    output_y = output_y.reshape(B, C, H, W)
    output_y = output_y/pixel_y

    return output_y
```

Differentials in p-direction (pressure levels direction) is implemented with PyTorch as follows:

```
def d_z(input_tensor):
```

```

conv_kernel = torch.zeros([1,1,5,1,1], device=input_tensor.device,
                           dtype=input_tensor.dtype,
                           requires_grad=False)

conv_kernel[0,0,0] = -1
conv_kernel[0,0,1] = 8
conv_kernel[0,0,3] = -8
conv_kernel[0,0,4] = 1

input_tensor = torch.cat((input_tensor[:, :2],
                           input_tensor,
                           input_tensor[:, -2:]), dim=1)

input_tensor = input_tensor.unsqueeze(1) # B, 1, C, H, W
output_z = F.conv3d(input_tensor, conv_kernel)/12
output_z = output_z.squeeze(1)
output_z = output_z/pixel_z.to(output_z.dtype).to(output_z.device)

return output_z

```

C Limitations and Future Work

The main limitation of our model is that only five important atmospheric equations are currently considered, which is still far from fully modeling the atmospheric motion process.

Another limitation of this paper is that the experiments have been conducted solely at a spatial resolution of 128×256 . As part of our future work, we plan to extend our experiments to higher resolutions such as 721×1440 to assess the model's performance under different settings. Additionally, while the minimum evolution time scale of our model is 15 minutes, we were unable to evaluate 15-minute generalized predictions due to the absence of corresponding validation data at that specific time scale. Therefore, we are currently only able to perform evaluations of 30-minute generalized predictions.

For future work, we plan to incorporate additional physical laws into our model and conduct higher-resolution experiments to ascertain the upper limit of its capabilities.